AIAA 80-1589R

Disturbance to the Launch of Fin-Stabilized Projectiles

Edward M. Schmidt*
ARRADCOM, Aberdeen Proving Ground, Md.

The sabot discard from a gun launched, fin-stabilized projectile is examined from the time of shot ejection until the round enters undisturbed flight. Trajectory perturbations due to muzzle blast, fin shadowing, mechanical contact, and aerodynamic interaction are evaluated and a relative ranking is determined. Analysis shows that muzzle blast and fin shadowing result in negligible changes to the launch angular momentum of the projectile; however, mechanical contact with sabot components markedly alters both the projectile momentum and the subsequent trajectory of the sabot sections. The resultant geometric asymmetry in the pattern of these discarding sections is shown to cause strong aerodynamic interaction between the sabot flowfields and the projectile. For the case investigated, aerodynamic interaction was determined to be the major source of post-separation trajectory perturbation.

Introduction

CURRENTLY, the most widely accepted design for kinetic energy, antitank applications is the sabot launched, fin-stabilized projectile. In order to be a viable candidate for the ground warfare role, a weapon system must be capable of achieving a high degree of precision. One contributing factor to precision is round-to-round dispersion.

For spin-stabilized projectiles, the most significant sources of dispersion originate either with gun induced mechanical interactions such as balloting, pointing error, throw off, tip off, etc., or with projectile inertial or aerodynamic asymmetries. However, with fin-stabilized designs, additional sources of launch perturbation may develop, Fig. 1. At ejection from the gun tube, the fins are exposed to the high velocity muzzle exhaust. With the fins in reverse flow, the projectile is statically unstable; yet, analysis of the region,[1] shows that the short residence period precludes the buildup of significant transverse velocities.

As the projectile penetrates the muzzle blast, the sabot components begin to move away from the flight body. During this process, the fins are in the wake of the sabot segments. This aerodynamic shadowing can decrease or even eliminate fin effectiveness resulting in static instability of the projectile.

At separation from the gun tube, the sabot and projectile are in direct mechanical contact. Elastic decompression, spin, and aerodynamic loadings act to lift the sabot components away from the projectile; however, mechanical interaction may persist if the components pivot about a point of contact with the body. Alternatively, the sabot components may initially break contact only to reimpinge on the projectile at a later stage in the discard. Asymmetries in the contact process can produce direct momentum transfer between the sabot segments and the projectile. Additionally, asymmetric momentum transfer, e.g., contact between the projectile and only one of the sabot components, can give rise to asymmetry in the sabot discard trajectories with respect to the flight body.

Geometric asymmetry in discard trajectories results in aerodynamic asymmetry in the mutually interacting flowfields associated with the sabot components and the projectile. This is the final type of launch disturbance considered. Experimental and analytical studies[2-4] have shown that interference loadings due to aerodynamic asymmetries may be significant.

The present paper will examine each of these possible sources of post ejection interaction: muzzle blast, fin shadowing, mechanical reimpingement, and aerodynamic interference. This examination is an extension of previous work[2] which concluded that aerodynamic interference was the only significant source of trajectory perturbation. The present analysis attempts to develop an order of magnitude estimate of the importance of the other potential sources of disturbance. The information source is firing data on a medium caliber, antitank projectile.

Experimental Apparatus and Test Procedure

The test projectile, Fig. 2, is fabricated from tungsten and has a diameter, *l*, of 23 mm, a length of 423 mm, and a fin span of 56 mm. A four segment aluminum sabot is employed to launch the round from a 60-mm tube which is rifled with

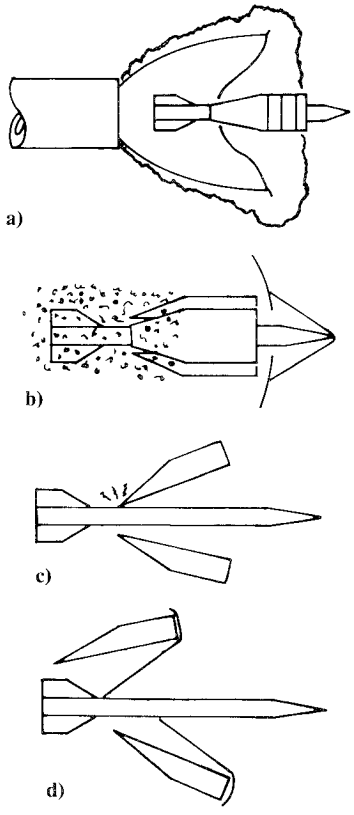

Fig. 1 Schematic of launch disturbances: a) muzzle blast, b) fin shadowing, c) mechanical contact, and d) aerodynamic asymmetry.

Presented as Paper 80-1589 at the AIAA 7th Atmospheric Flight Mechanics Conference, Danvers, Mass., Aug. 11-13, 1980; submitted Oct. 14, 1980; revision received June 1, 1981. This paper is declared a work of the U.S. Government and therefore is in the public domain.

*Aerospace Engineer, Ballistic Research Laboratory. Associate Fellow AIAA.

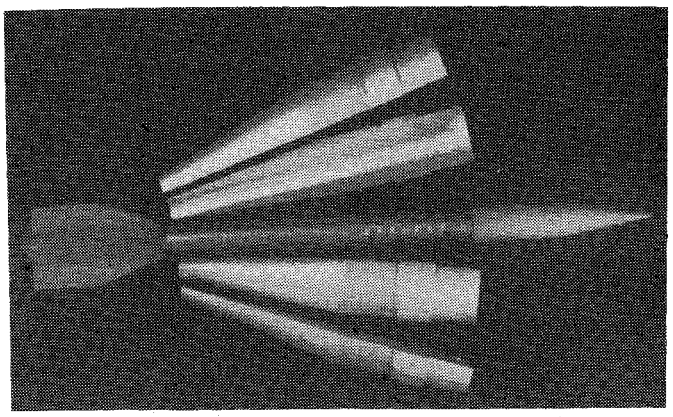

Fig. 2 Test projectile with sabot components.

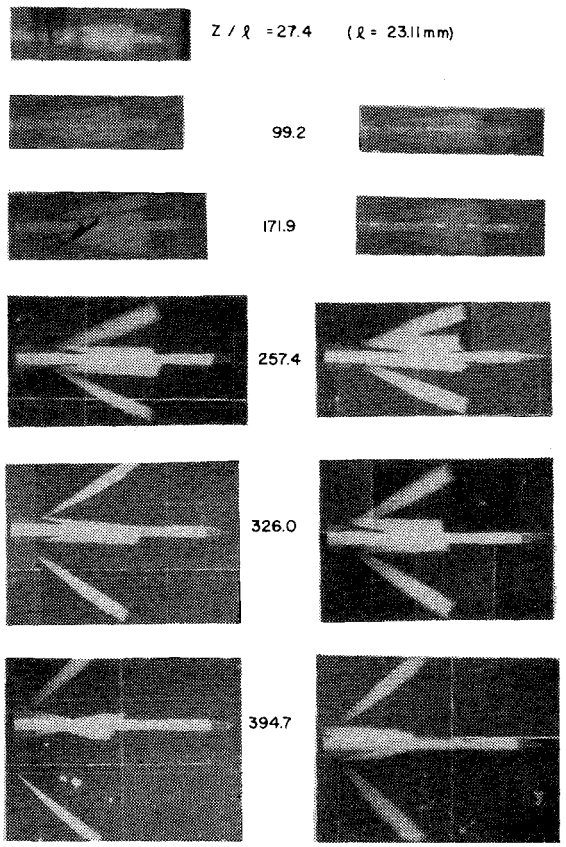

Fig. 3 X-ray photographic sequence of sabot discard.

one turn in 200 calibers of projectile travel. The launch velocity is 1310 m/s, and the initial roll rate is 110 rev/s.

Tests were conducted at the BRL Transonic Range using a combination of orthogonal x-ray stations near the muzzle and orthogonal spark shadowgraph stations within the range. Six x-ray stations are located at 1.7 m intervals over the first 9.0 m of the trajectory. These provide photographs of the sabot component and projectile motion during the period wherein strong interactions occur. Five smear cameras set at 4.6 m intervals measure the late stages of sabot discard. At 35 m from the muzzle, the round enters the Transonic Range where its yawing motion is measured at 25 spark shadowgraph stations extending from 40 to 200 m forward of the muzzle. This data provides information both on the launch disturbances and on the projectile aerodynamic characteristics. The latter are:

$$M_\infty = 3.91 \quad C_{L_\alpha} = 10.1 \quad C_{M_\alpha} = -21.5 \quad C_D = 0.46$$

The details of the data reduction procedure and the use of the x-ray and Transonic Range data to define the magnitude

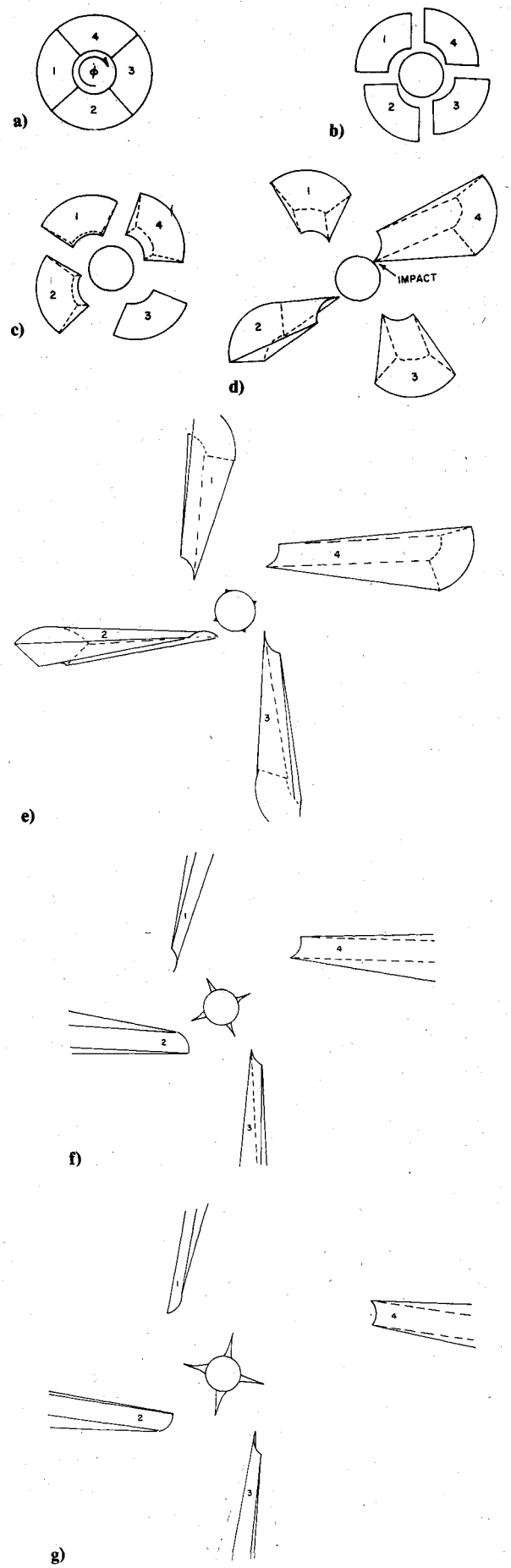

Fig. 4 Reconstructed rear view of sabot discard: a) $Z/l=0$; b) $Z/l=27.4$; c) $Z/l=99.2$; d) $Z/l=171.9$; e) $Z/l=257.4$; f) $Z/l=326.0$; g) $Z/l=394.7$.

of the sabot discard interactions relative to inbore disturbances are described in Ref. 2. In the present paper, only the x-ray photographs will be used to examine the sabot discard and resultant interactions. The smear camera photographs show that after 11.0 m of travel, the sabot components are sufficiently separated from the flight body to preclude any further interaction. Thus, the x-ray results, extending over the first 9.0 m of the trajectory, should provide adequate representation of the sabot discard dynamics.

Sabot Discard

Ten rounds were fired in the test program. Of these, eight complete sets of orthogonal x-rays were obtained. Analysis of this data showed that, contrary to previous statements,[2] two rounds had identifiable secondary mechanical contact followed by significant modifications to their yawing motion apparently due to aerodynamic interference. The remainder of the rounds did not display mechanical contact; however, the other sources of launch perturbation, Fig. 1, could be observed or inferred to have occurred. The rounds which left the gun tube with low values of angular rate had the greatest potential for secondary sabot component hits. This is possibly due to the nature of in-bore vibration of the projectile within its sabot. The low angular rate would be associated with a maximum of in-bore yaw (on the order of 0.1 deg). At such a maximum of yaw, the lateral stress within sabot components would be asymmetric and at its peak value. Upon separation, elastic decompression would occur differentially and produce variable initial dynamics for each sabot component, resulting in higher probability of preferential secondary impact. Rounds launched with high values of angular rate would be associated with a minimum of in-bore yawing motion wherein the differential stress in the sabot components would be relieved. However, rounds launched with high values of angular rate do display subsequent aerodynamic interference. In these cases, the large yaw angles attained by the projectile relative to the symmetrically discarding sabot components result in lateral aerodynamic loads.

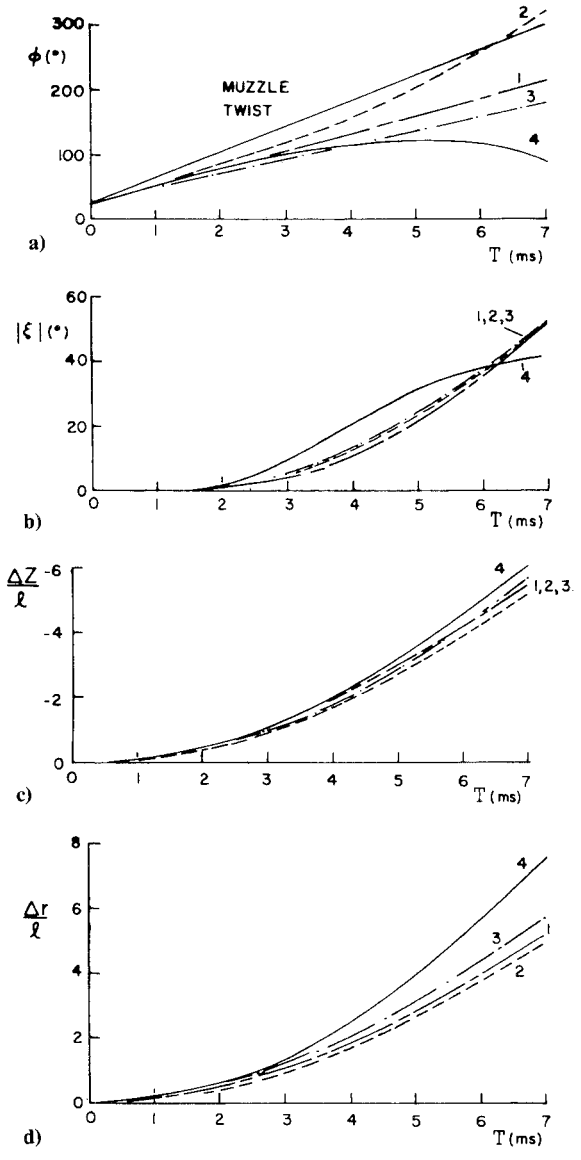

Fig. 5 Sabot component motion vs time: a) roll angle; b) yaw angle; c) axial displacement; d) radial displacement.

For the remainder of this paper, the launch perturbations to one of the eight data rounds which experienced secondary impact with a sabot component are addressed in detail. From the analysis of the projectile launch trajectory, an estimate of the order of magnitude of each source of disturbance, Fig. 1, compared to in-bore perturbations is developed. While it is not possible to generalize these results to treat the actual contribution to dispersion from each source, their relative importance can be assessed.

The orthogonal x-rays for the sample round are shown in Fig. 3. At the first station, the only observable motion is the shedding of the plastic centering and obturating bands and a slight lateral motion of the sabot components. Examination of the constructed rear view of the discard sequence, Fig. 4, shows that this lateral motion is largely due to the initial roll rate of the round. In the second set of x-rays, no significant pitch of the sabot segments is apparent. This station is located at 2.3 m from the muzzle. The projectile remains in the muzzle blast for the first 1.5 m of flight; thus, by the second station, the round has not been exposed to free flight aerodynamic loads for sufficient time to induce noticeable motion.

By the third x-ray station, the aerodynamic loads on the front chamfer of the sabot have caused the sabot components to pitch away from the flight body. Subsequent x-ray photographs show the continuation of this pitching motion and associated lateral displacement of sabot component centers of gravity. Since the components assume a high drag attitude and have relatively low mass, they begin to decelerate and fall behind the projectile.

While not obvious in the x-ray photographs, Fig. 3, an impact between the projectile and sabot component number 4 is observed in reconstructed geometry measured at the third station, Fig. 4. The effect of this impact is demonstrated in the remaining x-ray photographs and their corresponding rear views. The lateral momentum transferred to the sabot component due to impact causes it to move more rapidly away from the projectile than do the other sabot components. As such, an asymmetry in the discard pattern is generated which becomes more apparent with each successive x-ray (note the motion of component number 4 in the vertical views). The resulting imbalance in aerodynamic loading due to this asymmetry in the flow geometry will be discussed in more detail in the following sections.

From the x-ray photographs, the motion of each of the sabot components can be measured, Fig. 5. The variation in roll angle, ϕ, with time, Fig. 5a, is quite interesting. The two sabot components which are launched in a horizontal attitude, numbers 1 and 3, show roll histories which are similar and have nearly constant rates; however, the remaining two components have roll histories which diverge in opposite senses. Component number 4 suffers impact with the rolling projectile. However, component number 2 shows a diverging roll rate which is not presently explained. The magnitude of the angle of yaw, $|\xi|$, Fig. 5b, varies consistently for all of the components with the exception of number 4. Again, the impact would be expected to create a pivot point about which the sabot component would be rotated by the aerodynamic

loadings. The effect of the higher yaw level of component number 4 is reflected in the displacement of its center of gravity, Fig. 5c. While all the components fall back relative to the projectile, component number 4 does so at a slightly faster rate. The final figure in this sequence, Fig. 5d, shows the lateral displacement of the sabot component centers of gravity relative to the assembled positions. In this figure, the resulting asymmetry due to impact is clearly indicated.

In the remainder of this paper, the launch disturbances to which this round is subject are analyzed and a relative ranking determined.

Analysis of Launch Disturbances

Muzzle Blast

The first possible source of perturbation subsequent to shot ejection is the muzzle blast. The magnitude of muzzle blast interaction may be estimated from the launch properties of the projectile measured by x-rays. Figure 6 shows the variation in projectile angle of attack, α, and angle of sideslip, β, as the round moves through the x-ray field of view. Each data point corresponds to a particular x-ray station. From these data, the initial launch properties of the round are estimated

$$|\xi_0| = 0.05 \text{ deg}, \qquad |\dot{\xi}_0| = 1.28 \text{ rad/s}$$

The magnitude of the angular rate of the projectile at shot ejection, $|\dot{\xi}_0|$, is taken as a parameter indicative of the transverse impulse imparted to the projectile both in-bore and during mechanical disengagement. This value will serve as the reference against which subsequent trajectory perturbations will be compared. As previously noted, the separation angular rates of the rounds which experience secondary impact were at the low end of the distribution.

The change in angular velocity due to the projectile passage through the muzzle blast may be computed[1] from:

$$|\Delta\dot{\xi}|_{\text{m.b.}} = (\gamma + 1) p^* (nA/2) (\delta D / I_y V_p) \bar{P} |\xi_0| \qquad (1)$$

where $\gamma = 1.25$, $p^* = 1.38 \times 10^8$ N/m^2, n is the number of fins $= 4$, A is the area of single fin $= 1.058 \times 10^{-3}$ m^2, δ is the c.p.-c.g. separation $= 0.16$ m, D is the gun tube diameter $= 0.06$ m, $I_y = 0.0192$ kg-m^2, V_p is the launch velocity $= 1310$ m/s, and $\bar{P}$ is the momentum transfer function $= 0.3$.

Substituting these values into Eq. (1) results in

$$|\Delta\dot{\xi}|_{\text{m.b.}} = 6.73 \times 10^{-2} \text{ rad/s}$$

or

$$|\Delta\dot{\xi}|_{\text{m.b.}} / |\dot{\xi}_0| \sim 5 \times 10^{-2}$$

indicating that the influence of muzzle blast is negligible.

Fin Shadowing

When the projectile penetrates the muzzle blast, it begins to experience flow from the forward direction; however, the sabot components are in close proximity to the round and tend to mask the fins in their wake. As such, the projectile may be statically unstable, and since the roll rate is low, the projectile is gyroscopically unstable. To determine the importance of fin shadowing as a source of dispersion, a comparison will be made of the projectile yawing motion under two conditions: 1) the fins are completely shadowed, and 2) the fins are not shadowed, i.e., normal free flight.

The solution to the equations of motion for a projectile executing small amplitude oscillations have been developed by Murphy.[5] A symmetric projectile executes an epicyclic yawing motion which may be described, in the complex plane, as

$$\xi = \beta + i\alpha = \sum_{j=1}^{2} k_{j_0} e^{i\phi_{j_0}} e^{(\lambda_j + i\phi'_j)s} \qquad (2)$$

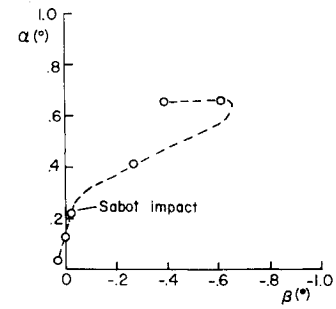

Fig. 6 Yawing motion of projectile measured from x-rays.

Since fin shadowing occurs near the weapon muzzle, examine the solution at $s = 0$,

$$\xi_0 = k_{1_0} e^{i\phi_{1_0}} + k_{2_0} e^{i\phi_{2_0}} \qquad (3)$$

$$\xi'_0 = (\lambda_1 + i\phi'_1) k_{1_0} e^{i\phi_{1_0}} + (\lambda_2 + i\phi'_2) k_{2_0} e^{i\phi_{2_0}} \qquad (4)$$

By assuming that $\xi_0 = 0$, the following relations may be obtained

$$k_{1_0} = k_{2_0} = K \qquad (5)$$

$$\phi_{1_0} = \phi_{2_0} + \pi \qquad (6)$$

If aerodynamic damping is neglected,

$$\lambda_j + i\phi'_j \cong (iP \pm [4M - P^2]^{1/2})/2 \qquad (7)$$

where

$$M = \rho S l^3 C_{M_\alpha} / 2I_y, \quad P = (I_x/I_y)(pl/V), \quad \rho = 1.21 \text{ kg/m}^3,$$

$$l = 0.02311 \text{ m}, \quad S = \pi l^2/4 = 4.19 \times 10^{-4} \text{ m}^2$$

$$I_x/I_y = 0.521 \times 10^{-2}, \quad pl/V = 1.21 \times 10^{-2} \text{ rad/cal}$$

Using Eqs. (5-7) in Eq. (4) yields

$$K = |\xi'_0| / (4M - P^2)^{1/2}$$

The aerodynamic moment is the single property which is different for the two conditions treated. With shadowing, it is assumed that only nose lift contributes to the overturning moment. Thus, for a conical nose in hypersonic flight, $C_{L_\alpha} = 2.0$ and the resulting overturning moment is $C_{M_\alpha} = +16.3$. Giving

$$\lambda_j + i\phi'_j = \pm 1.63 \times 10^{-3} + i3.15 \times 10^{-5}$$

with a yawing motion of the form

$$\xi = K e^{i\phi_0} e^{i\phi' s} (e^{+\lambda s} - e^{-\lambda s}) \text{ (case 1)} \qquad (8)$$

For normal free flight, $C_{M_\alpha} = -21.5$ and

$$\lambda_j + i\phi'_j = +i\,1.90 \times 10^{-3}; \quad -i\,1.84 \times 10^{-3}$$

with

$$\xi = K e^{i\phi_0} (e^{i\phi'_1 s} - e^{i\phi'_2 s}) \text{ (case 2)} \qquad (9)$$

The two types of motion are quite different. In case 1, fin shadowing produces instability. The yaw angle can be described as a two-armed motion, both having rotation in the same direction at the same velocity. However, the size of one of the arms is damped while that of the other grows without bound. In case 2, the normal free flight motion is bounded and consists of a two-armed motion having equal magnitudes but rotating in opposite directions at slightly different rates.

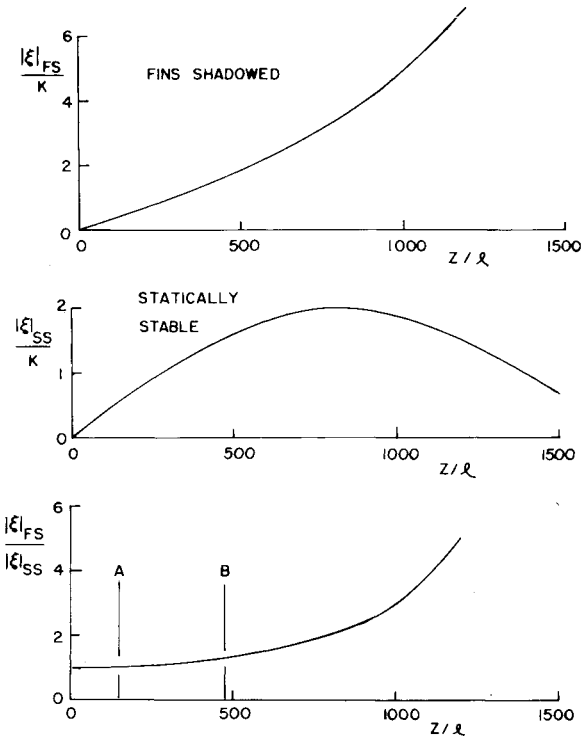

Fig. 7 Comparison of yaw of fin-shadowed and statically stable projectile vs distance from muzzle.

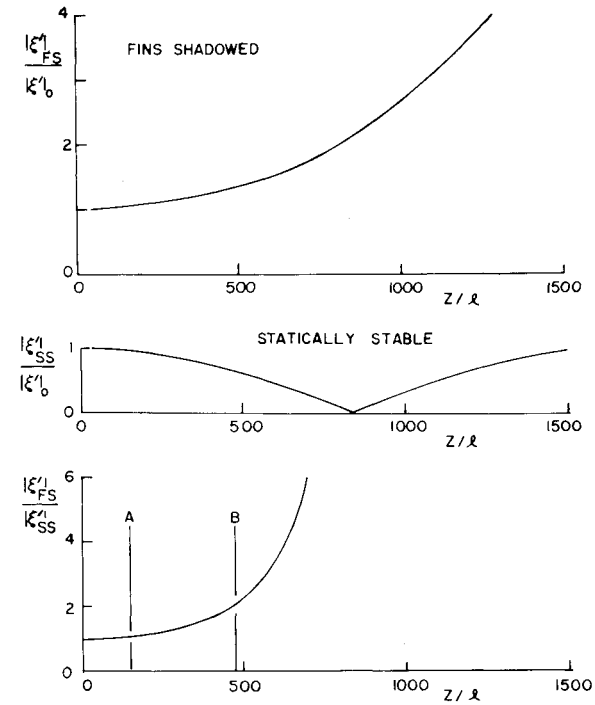

Fig. 8 Comparison of yawing velocity of fin-shadowed and statically stable projectile vs distance from muzzle.

From Eqs. (8) and (9), the normalized initial yaw and yawing velocity are computed for both cases, Figs. 7 and 8. As anticipated for case 1, both grow without bound while the motion for case 2 is typical of a statically stable round. The lower curve on each of the figures gives the ratio of the motions. The sabot components can aerodynamically interact with the projectile over the first 11.0 m of flight (Limit B, $Z/l=475$). In this range, the angle of yaw does not grow appreciably; however, the yawing velocity of the shadowed projectile is twice that which would have occurred if normal free flight aerodynamics were in effect. Obviously, the fins are not shadowed during the complete discard process.

A better estimate of the shadowing distance can be made by considering the sabot discard analysis of Siegelman et al.[6] They postulate that the flow between the sabot segments remains choked until the area becomes sufficiently large to pass the mass flow taken in by the inlet scoops (i.e., analogous to a supersonic inlet, the sabot leading edges entrain the air stream which is forced out either around the edges or between the segments). For the freestream conditions of the present test; $M_\infty=3.91$, the conditions behind the inlet (normal) shock are

$$M_2=0.44, \qquad A/A^*=1.47$$

The swallowing area ratio is developed when the sabot separates 20.2 mm from the flight body. Figure 5d shows this standoff, $\Delta r/l=0.87$, occurs by 2.5 ms into the flight; therefore, $Z/l=142$, Limit A, Fig. 7.

This value is presumed to be a more realistic estimate of the extent of possible fin shadowing. The resulting growth in either yaw or yawing velocity by $Z/l=142$ is seen to be rather small, Figs. 7 and 8, and

$$|\Delta\dot{\xi}|_{f.s.}/|\dot{\xi}_0| \sim 5\times 10^{-2}$$

Thus, for a round which has rapid sabot discard, it may be concluded that the effect of fin shadowing by the discarding sabot components is not significant.

Mechanical Contact

Direct contact between sabot components and the flight body during discard results in momentum exchange which alters the trajectories of both the projectile and the sabot segment. The sabot component motion during and subsequent to impact has been discussed previously. In this section, the momentum imparted to the projectile will be examined.

The yawing motion of the projectile is plotted in Fig. 6. The initial angular velocity of the round is fairly low (indicated by the variation in angle between data points which are taken at roughly 1.3-ms intervals); however, after the impact occurs, the angular velocity changes in both magnitude and orientation. From Fig. 4, the impact between the projectile and sabot component number 4 is taking place on the upper right-hand quadrant behind the projectile center of gravity. The resulting moment would push the aft of the projectile downward and to the left. In turn, the nose of the projectile moves upward and toward the right, i.e., direction of increasingly positive angle of attack α and increasingly negative angle of sideslip β, Fig. 6. By plotting these angles vs time of flight, the alteration in yawing velocities may be estimated

$$\Delta\dot{\alpha}=2.45 \text{ rad/s}, \qquad \Delta\dot{\beta}=-6.95 \text{ rad/s}$$

thus,

$$|\Delta\dot{\xi}|/|\dot{\xi}_0| \sim 6$$

While the angles involved in the measurement are quite small and the accuracy of differencing data is always questionable, the order of magnitude of the momentum exchange due to impact is sufficiently large to indicate that it is a significant contributor to the transverse launch perturbation. The secondary contribution of the impact, discard asymmetry, will be analyzed next.

Aerodynamic Interference

The nature of the flowfield associated with an asymmetric discard geometry of sabot components is illustrated by the spark shadowgraph of Fig. 9. A fin-stabilized model is seen flying with the two remaining segments of an originally four segment sabot. The flowfield is highly asymmetric. The strong shock wave from the upper sabot segment impinges roughly 3 calibers up on the body, whereas, the shock wave from the lower sabot segment is seen to intersect very near the base. The resulting pressure distribution induced by the shock impingements would produce a strong overturning moment.

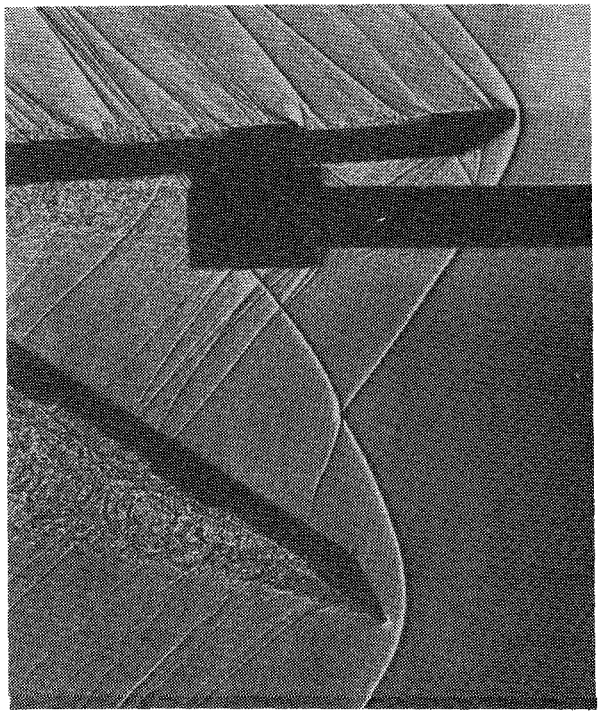

Fig. 9 Spark shadowgraph of asymmetric sabot discard.

Similar asymmetries develop in the flowfield surrounding the current projectile due to the irregular sabot discard geometry for the case under consideration, Figs. 3 and 4. The effect of the aerodynamic loads upon the projectile motion is seen in Fig. 6. Rather than following a yawing history compatible with the response to the mechanical impact (i.e., in undisturbed flight the projectile yaw would grow monotonically to a first maximum yaw 19 m after being hit[2]), the projectile reaches an extremum of yaw only two stations (3.5 m) from the point of impact. This shortening of the yawing period is caused by aerodynamic interference between the projectile and sabot component flowfields. To demonstrate that the measured motion is compatible with aerodynamic loadings, the flowfield model proposed in Ref. 2 will be used.

Rather than treating the sabot segments as fully three-dimensional bodies, they are approximated as two-dimensional wedges. The wedge apex location and half-angle are determined from the x-ray photographs. Oblique shock wave compatible with the freestream Mach number and wedge angle are projected to the projectile. The shocks are reflected at the body either as weak shocks or normal shocks according to the local flow conditions. Cross flow around the body is neglected as are the details of shock intersections. Since the sabot geometry in the vertical plane was approximately symmetric, the transverse moment acts only in the horizontal plane. Taking as initial conditions the projectile state following impact and using the measured sabot trajectories, the equation of motion may be integrated to determine the resulting variation in yaw angle, Fig. 10.

Due to the gross assumptions regarding the flowfield, the prediction overestimates the angular acceleration induced by

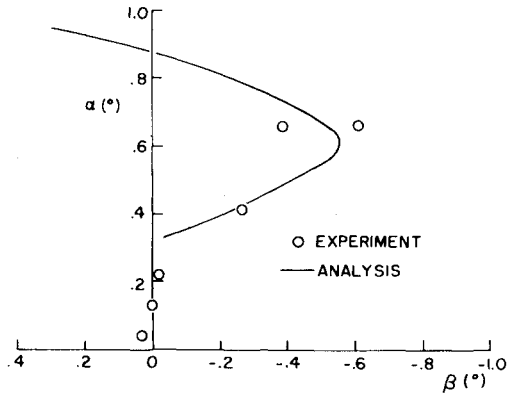

Fig. 10 Projectile motion predicted by flow interference model.

aerodynamic loads. However, the comparison between predicted and measured acceleration is sufficiently good to use the analysis to determine the order of magnitude of the impulse due to aerodynamic interference. Integrating the angular acceleration over the period of interaction provides:

$$|\Delta\dot{\xi}|_{a.i.} / |\dot{\xi}_0| = 23$$

This indicates that the aerodynamic interference is an important source trajectory perturbation.

Summary and Conclusions

A set of possible perturbations to the trajectory of a fin-stabilized projectile is identified. Each source occurs after the round has separated from the gun tube. Previous research[2-4] has demonstrated that the impulse imparted to sabot launched, fin-stabilized projectiles following separation from the gun tube can be of the same order of magnitude as that imparted in-bore and during mechanical disengagement. The present results are used to assess the contribution of the identified sources of perturbation to the overall impulse. Muzzle blast and fin shadowing effects are two orders of magnitude less severe, while mechanical contact and aerodynamic interference can be of the same order of magnitude as the in-bore impulse.

References

[1] Schmidt, E.M., Fansler, K.S., and Shear, D.D., "Trajectory Perturbations of Fin-Stabilized Projectiles due to Muzzle Blast," *Journal of Spacecraft and Rockets,* Vol. 14, June 1977, pp. 339-344.

[2] Schmidt, E.M. and Shear, D.D., "Aerodynamic Interference During Sabot Discard," *Journal of Spacecraft and Rockets,* Vol. 15, May-June 1978, pp. 162-167.

[3] Conn, H., "The Influence of Sabot Separation on the Yawing Motion of a Cone," Defense Research Establishment, Valcartier, Canada, Technical Report 1849/70, June 1970 (AD 880697L).

[4] Glauz, W.D., "Estimation of Forces on a Flechette Resulting from a Shock Wave," Midwest Research Institute, Kansas City, Mo., R3451-E, May 1971 (AD 724178).

[5] Murphy, C.H., "Free Flight Motion of Symmetric Missiles," BRL Report 1216, Ballistic Research Laboratory, Aberdeen Proving Ground, Md., July 1963 (AD 442757).

[6] Siegelman, D., Crimi, P., and Schmidt, E.M., "Projectile/Sabot Discard Aerodynamics," AIAA Paper 80-1588, Aug. 1980.